

## Article

# Sulfur Isotope and Stoichiometry–Based Source Identification of Major Ions and Risk Assessment in Chishui River Basin, Southwest China

Xin Ge <sup>1</sup>, Qixin Wu <sup>1,\*</sup>, Zhuhong Wang <sup>2</sup>, Shilin Gao <sup>1</sup> and Tao Wang <sup>1</sup>

<sup>1</sup> Key Laboratory of Karst Geological Resources and Environment, College of Resources and Environmental Engineering, Guizhou University, Guiyang 550025, China; april\_gexin@163.com (X.G.); gaoshilin110@163.com (S.G.); wangtao6090@126.com (T.W.)

<sup>2</sup> Key Laboratory of Environmental Pollution and Disease Monitoring of Ministry of Education, School of Public Health, Guizhou Medical University, Guiyang 550000, China; cindywzh@163.com

\* Correspondence: qxwu@gzu.edu.cn

**Abstract:** Hydrochemistry and sulfur isotope ( $\delta^{34}\text{S}\text{-SO}_4^{2-}$ ) of Chishui River watershed in Southwest China were measured to identify the sources of riverine solutes, the potential impact of human activities, water quality, and health risk. The main findings indicated that the  $\text{HCO}_3^-$  (2.22 mmol/L) and  $\text{Ca}^{2+}$  (1.54 mmol/L) were the major ions, with the cation order of  $\text{Ca}^{2+}$  ( $71 \pm 6\%$ ) >  $\text{Mg}^{2+}$  ( $21 \pm 6\%$ ) >  $\text{Na}^+ + \text{K}^+$  ( $8 \pm 3\%$ ) and the anion sequence of  $\text{HCO}_3^-$  ( $55 \pm 9\%$ ) >  $\text{SO}_4^{2-}$  ( $41 \pm 9\%$ ) >  $\text{Cl}^-$  ( $4 \pm 3\%$ ). The riverine  $\delta^{34}\text{S}\text{-SO}_4^{2-}$  values fluctuated from  $-7.79\%$  to  $+22.13\%$  (average  $+4.68\%$ ). Overall, the water samples from Chishui River presented a hydrochemical type of Calcium–Bicarbonate. The stoichiometry and PCA analysis extracted three PCs that explained 79.67% of the total variances. PC 1 with significantly positive loadings of  $\text{K}^+$ ,  $\text{Mg}^{2+}$ ,  $\text{F}^-$ ,  $\text{HCO}_3^-$  and relatively strong loading of  $\text{Ca}^{2+}$  revealed the natural sources of rock weathering inputs (mainly carbonate). PC 2 ( $\text{Na}^+$  and  $\text{Cl}^-$ ) was primarily explained as atmospheric contribution, while the human inputs were assuaged by landscape setting and river water mixing processes. The strongest loadings of  $\text{SO}_4^{2-}$  and  $\text{NO}_3^-$  were found in PC 3, which could be defined as the anthropogenic inputs. The  $\text{H}_2\text{SO}_4$ –involved weathering processes significantly impacted (facilitated weathering) the concentrations of riverine total ions. Sulfur isotope compositions further indicated that riverine  $\text{SO}_4^{2-}$  were mainly controlled by anthropogenic inputs  $\text{SO}_4^{2-}$  compared to the sulfide oxidation derived  $\text{SO}_4^{2-}$ , and the atmospheric contribution was very limited. The results of risk and water quality assessment demonstrated that Chishui River water was desirable for irrigation and drinking purposes due to low hazard quotient values ( $<1$ , ignorable risk), but long–term monitoring is still worthy under the circumstances of global environmental change.

**Keywords:** water chemistry; sulfur isotope; ion source apportionment; water quality and risk assessment; Chishui River watershed



**Citation:** Ge, X.; Wu, Q.; Wang, Z.; Gao, S.; Wang, T. Sulfur Isotope and Stoichiometry–Based Source Identification of Major Ions and Risk Assessment in Chishui River Basin, Southwest China. *Water* **2021**, *13*, 1231. <https://doi.org/10.3390/w13091231>

Academic Editor: Frédéric Huneau

Received: 22 March 2021

Accepted: 25 April 2021

Published: 28 April 2021

**Publisher's Note:** MDPI stays neutral with regard to jurisdictional claims in published maps and institutional affiliations.



**Copyright:** © 2021 by the authors. Licensee MDPI, Basel, Switzerland. This article is an open access article distributed under the terms and conditions of the Creative Commons Attribution (CC BY) license (<https://creativecommons.org/licenses/by/4.0/>).

## 1. Introduction

Watershed–scale hydrochemical evolution and water environmental quality, the most important hot point for river water resource research, is the basis of effective hydrospheric environment planning and sustainable usage of freshwater resources, in particular, under the background of the imbalance between unevenly distributed water resources and water requirements. Both anthropogenic and natural processes can affect hydrochemistry and the major ion concentration level [1,2]. With the accelerated improvement of economy, the increased anthropogenic activities (e.g., industrial/domestic wastewater, agricultural emissions) have rapidly enhanced the riverine pollutants [3,4], which will further result in a series of environmental issues and risks [5,6], such as the destruction of soil aggregate structure by polluted river water irrigation, and the health risks via drinking water [7–9].

The major ions are the most important part of river dissolved loads. Exploring the origins of these ions could greatly benefit for the understanding of watershed-scale geochemical dynamics (e.g., weathering processes) and distribution/transformation regulation of pollutants. Moreover, the ion source identification is also benefit for the environmental supervision of the government [10]. Generally, in addition to regularly direct monitoring of cation and anion concentrations, statistic approaches, ion ratios, and isotopic methods are widely applied in source identification [11]. Statistical methods, such as principal component analysis and correlation analysis could explore the common sources of riverine solutes due to similar physicochemical characteristics and potential co-origins of some ionic species [12]. The potential dilution effect can be avoided by the fluvial ion ratios, reflecting the mixing processes of the sources [13]. The isotopic methods, such as sulfur (S) isotope of riverine  $\text{SO}_4^{2-}$ , could distinguish different sources via specific isotope compositions of these end-members, based on the inheritance of S isotopes of riverine sulfate from both natural and anthropogenic sources [2,14].

In the karst area of southwest China, the typical carbonate geomorphology is developed, such as the sinkhole, depression, cockpit, and cone, which further result in the barren and thin soil [15,16]. Thus, the karstic ecosystem, in particular river system is extremely sensitive and vulnerable due to the unique geological conditions and strong karstification [17,18]. In order to obtain more knowledge of karst fluvial hydrochemistry, this study presents the detailed investigation of river water stoichiometry and S isotope of Chishui River (a tributary of upper Yangtze River) watershed in southwest China karst region. The main aims are to:

- (i) Clarify the ionic compositions and S isotope compositions of river water,
- (ii) identify the source of major ions, and
- (iii) explore the water quality as well as the potential irrigation and health risks.

## 2. Materials and Methods

### 2.1. Study Region

The Chishui River is one of the first-level tributaries in upper Yangtze River that has not been dammed in the main channel. With a total length of 445 km for main stream, the Chishui River begins in the Zhenxiang County, Yunnan Province and flows from southwest to northeast through Yunnan-Guizhou Plateau and Sichuan Basin in southwestern China, and finally enters into the Yangtze River in Hejiang County, Sichuan Province (Figure 1) [7]. In Chishui River watershed (CRW,  $27^{\circ}15' \sim 28^{\circ}50' \text{ N}$ ,  $104^{\circ}44' \sim 107^{\circ}1' \text{ E}$ ), there is a wide catchment area ( $\sim 1.89 \times 10^4 \text{ km}^2$ ) with various tributaries influenced by different degrees of human activities. As shown in Figure 1a, the lithology exposed in CRW is mainly composed of carbonate sedimentary rocks ( $\sim 44.6\%$ ), siliciclastic sedimentary rocks ( $\sim 24.5\%$ ), mixed sedimentary rocks ( $\sim 30.1\%$ ), and basic volcanic rocks ( $\sim 0.7\%$ ). In more detail, the strata distributed in upper stream are mainly dolomite of Dengying Formation of Ediacaran with the minerals resources of phosphorite, barite, and fluorite. The middle reaches are mainly composed of limestone and dolomite of Cambrian, Ordovician, Silurian, Permian, Triassic, and Jurassic, followed by mudstone, sand shale and coal-bearing rock group. The middle reaches also developed the minerals resources of coal, pyrite (iron sulfide), gypsum, and barite with the same geological age. The lower stream mainly distributed Jurassic-Cretaceous siltstone and mudstone with sporadic oil shale. The CRW covers various land use and a large elevation range (205 to 2237 m). The land use of CRW mainly includes water area, urban area, grass land, unused land, cropland, and forest land (Figure 1b). Forest land ( $\sim 73.4\%$ ) and cropland ( $\sim 19.6\%$ ) are the dominant land uses in CRW. The CRW is affected by the sub-tropical monsoon climate, with the average annual air temperature of  $11 \sim 13^{\circ} \text{ C}$ . The annual rainfall ranges from 800 to 1200 mm. The agriculture is distributed in upper-middle stream with a vulnerable eco-environment, while the industries are mainly located in the middle stream. The water quality of CWR is of great importance due the significant supporting role of water resources in the watershed.

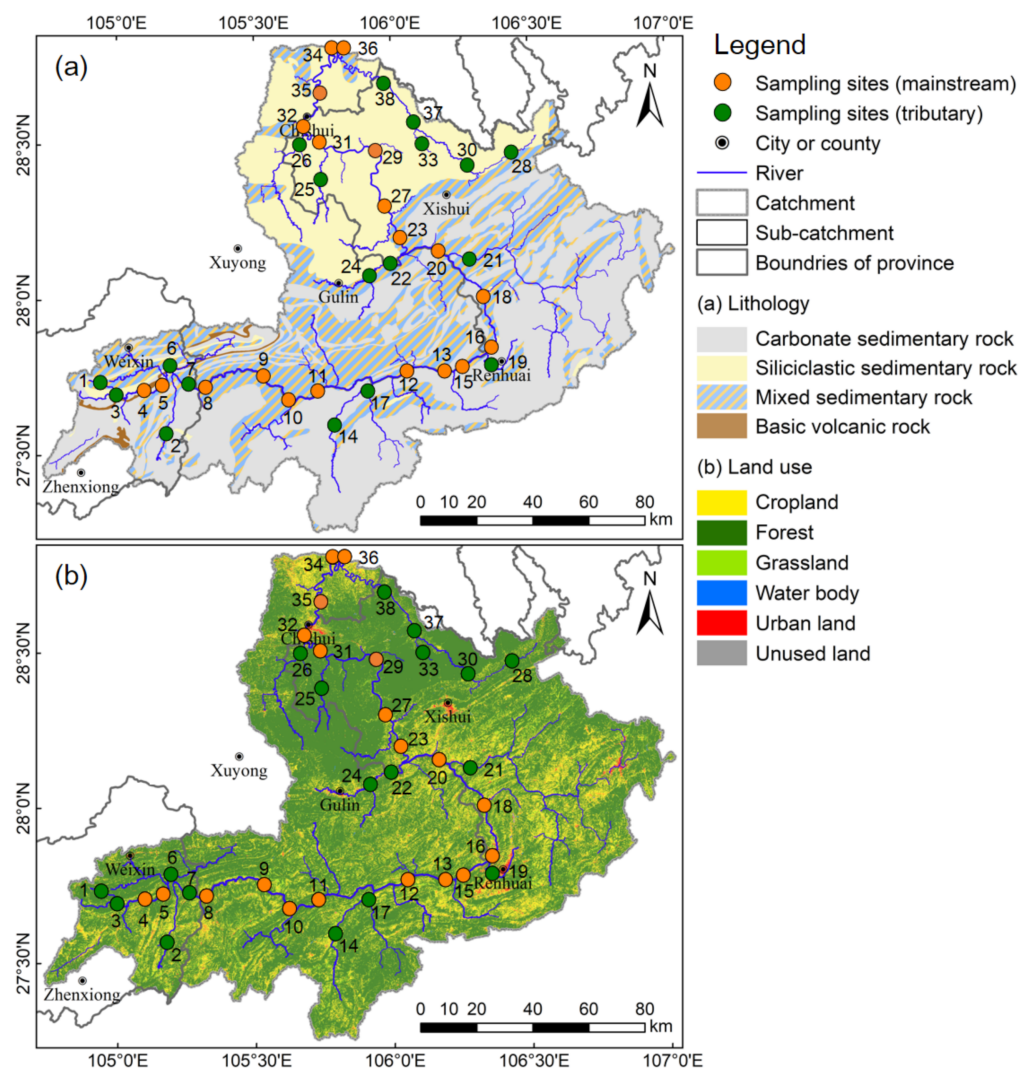


**Figure 1.** The background of sampling sites: (a) the lithology distribution of Chishui River watershed; (b) the land use of Chishui River watershed.

## 2.2. Sample Collection and Analyses

A systematic watershed survey was conducted from November to December in 2012 (dry season was selected to avoid the dilution effect and biologic effect as much as possible). According to the natural features (landuse and lithology) and the population distribution, 38 sample sites were chosen in the mainstream and tributaries of CRW (2 sites were chosen in Changjiang River, Figure 1). In total, 38 river water samples were obtained and further filtered (0.45- $\mu\text{m}$  membrane, Millipore) and saved in the clean polyethylene sample bottles. Each sample was divided into three parts for the measurement of sulfur isotope and the major ions. The storage conditions of all samples were lightless and refrigerated (4 °C). The river water parameters (pH, T, DO, and EC) were measured in the field using the multi-parameter meter (Multi Line 3320, WTW, Munich, Bavaria, Germany).  $\text{HCO}_3^-$  concentrations were detected by HCl-titrated method. The  $\text{Na}^+$ ,  $\text{K}^+$ ,  $\text{Mg}^{2+}$ ,  $\text{Ca}^{2+}$ ,  $\text{F}^-$ ,  $\text{Cl}^-$ ,  $\text{NO}_3^-$ , and  $\text{SO}_4^{2-}$  concentrations were measured by ion chromatograph (ICS-1100, Thermo Fisher, Waltham, MA, USA) at the Key Laboratory of Karst Geological Resources and Environment, Ministry of Education, Guizhou University. The analysis was conducted with replicate samples and procedural blanks to maintain the accuracy of measurement. The measured result of replicate samples suggested acceptable repeatability for all ions (relative standard deviations were within  $\pm 5\%$ ), and the procedural blanks for all ions were generally lower than the detection limit.

The sulfur isotope of riverine  $\text{SO}_4^{2-}$  was detected according to previous studies [19]. Briefly, 10%  $\text{BaCl}_2$  solution were added to water samples to convert the dissolved  $\text{SO}_4^{2-}$  into  $\text{BaSO}_4$  precipitation, and the mixture was filtered by 0.45- $\mu\text{m}$  membrane filters after 48 h. Then, the  $\text{BaSO}_4$  precipitation on membranes was further calcined (800 °C, 40 min) to gain the  $\text{BaSO}_4$  solid. The S isotope compositions (in  $\delta$  notation relative to Vienna–Canyon Diablo Troilite, VCDT; Equation (1)) were detected by Elemental Analyzer–IsoPrime MS (IsoPrime, GV Instruments, Manchester, UK) at the Institute of Geochemistry, Chinese Academy of Sciences [20].

$$\delta^{34}\text{S} (\text{‰}) = (R_{\text{sample}}/R_{\text{VCDT}} - 1) \times 1000 \quad (1)$$

The standard reference materials (NBS 127) and internal laboratory standard reference materials (pre-calibrated Lab-SO1, Lab-SO4, Lab-Sigma) for S isotope were also detected to ensure the analysis accuracy, which were within the recommended value (2SD smaller than 0.02‰).

### 2.3. Assessment Method

Chishui River is the most important water source of both drinking and agricultural irrigation water within the watershed, which is necessary to assess the suitability for drinking and irrigation purpose. The riverine parameters (pH) and ion concentrations of Chishui River water were appraised by Chinese (GB 5749–2006) and WHO drinking water quality guidelines. For the irrigation water quality, the soil quality attributes can be influenced by the different salinity and alkalinity level of irrigation water, and further changed the yields from farmland. To gain an overall evaluation of irrigation water salinity and alkalinity hazard, the commonly-applied indicators such as sodium adsorption ratio (SAR), soluble sodium percentage (Na%), and residual sodium carbonate (RSC) were calculated based on the ion equivalent concentrations (meq/L) of river water as follows [11]:

$$\text{SAR} = \text{Na}^+ \times [2/(\text{Mg}^{2+} + \text{Ca}^{2+})]^{0.5} \quad (2)$$

$$\text{Na}\% = 100\% \times \text{Na}^+ / (\text{Na}^+ + \text{K}^+ + \text{Mg}^{2+} + \text{Ca}^{2+}) \quad (3)$$

$$\text{RSC} = (\text{HCO}_3^- + \text{CO}_3^{2-}) - (\text{Mg}^{2+} + \text{Ca}^{2+}) \quad (4)$$

Regarding to the human health risk, the health threat could be occurred via ingestion and dermal exposure to river water with high-concentration ions [21]. In comparison, the health risk through ingestion intake is the most noteworthy. To assess this threat (non-carcinogenic health risk), the Hazard quotient (HQ) suggested by the U.S. Environmental Protection Agency was calculated for  $\text{F}^-$ ,  $\text{NO}_3^-$ , and  $\text{NH}_4^+$  [11]:

$$\text{ADD}_{\text{ingestion}} = C \times \text{IR} \times \text{EF} \times \text{ED} / (\text{BW} \times \text{AT}) \quad (5)$$

$$\text{HQ} = \text{ADD} / \text{RfD} \quad (6)$$

where  $\text{ADD}_{\text{ingestion}}$ , C, IR, EF, ED, BW, AT, and RfD represents the daily ingestion intake doses, ion concentrations (mg/L), daily ingestion rate (0.6 L/day for children, 1.0 L/day for adults), exposure frequency (365 days/year), exposure duration (12 and 25 years for children and adults), body weight (16 and 56 kg for children and adults), average time for non-carcinogenic effect (4380 and 10950 days for children and adults), reference dose of different ions (0.04, 1.6, and 0.97 ppm/day for  $\text{F}^-$ ,  $\text{NO}_3^-$ , and  $\text{NH}_4^+$ ), respectively. If the HQ of each ion (or total hazard quotient,  $\text{HQ}_t$ ) is >1, the local people will be threatened by the corresponding ion-derived risk.

### 2.4. Software for Data Analyses

For the statistical analyses of riverine ion concentrations and other parameters, the principal component analysis (PCA, a common method for exploring the potential origins

of ions) and Piper diagram analysis were carried out by SPSS 21.0. All the data-based figures were illustrated by Origin 2018.

### 3. Results and Discussion

#### 3.1. Overview of Hydrochemical Compositions

The hydrochemical compositions and parameters of all river water samples are presented in Table S1, with the statistical results, including ranges, and mean values of these data summarized in Table 1. The pH values ranged from 7.63 to 8.87 (mean value 8.35), presenting the slightly alkaline river waters, further indicated that the inorganic carbon species was dominated by bicarbonate ( $\text{HCO}_3^-$ ) based on the carbonate equilibrium, while  $\text{CO}_3^{2-}$  and dissolved  $\text{CO}_2$  were negligible. The EC value averaged 403  $\mu\text{S}/\text{cm}$  with a range of 128–738  $\mu\text{S}/\text{cm}$ . The ionic balance was also applied for the river water samples, that is, the total cation concentration ( $\text{TZ}^+ = \text{Na}^+ + \text{K}^+ + \text{Mg}^{2+} + \text{Ca}^{2+}$ , in meq/L) and total anion concentration ( $\text{TZ}^- = \text{F}^- + \text{Cl}^- + \text{NO}_3^- + \text{SO}_4^{2-} + \text{HCO}_3^-$ , in meq/L) of river water, which presented well ion balances ( $R^2 = 0.987$ ,  $p < 0.01$ ). The normalized ionic charge balance ( $[\text{TZ}^+ - \text{TZ}^-]/\text{TZ}^-$ ) is smaller than 11% (Table S1), suggesting the potential effect of the organic anionic species [22] like oxalate.

**Table 1.** Statistical result of hydrochemical compositions, parameters,  $\delta^{34}\text{S}$  values, SAR, Na%, and RSC of Chishui River water.

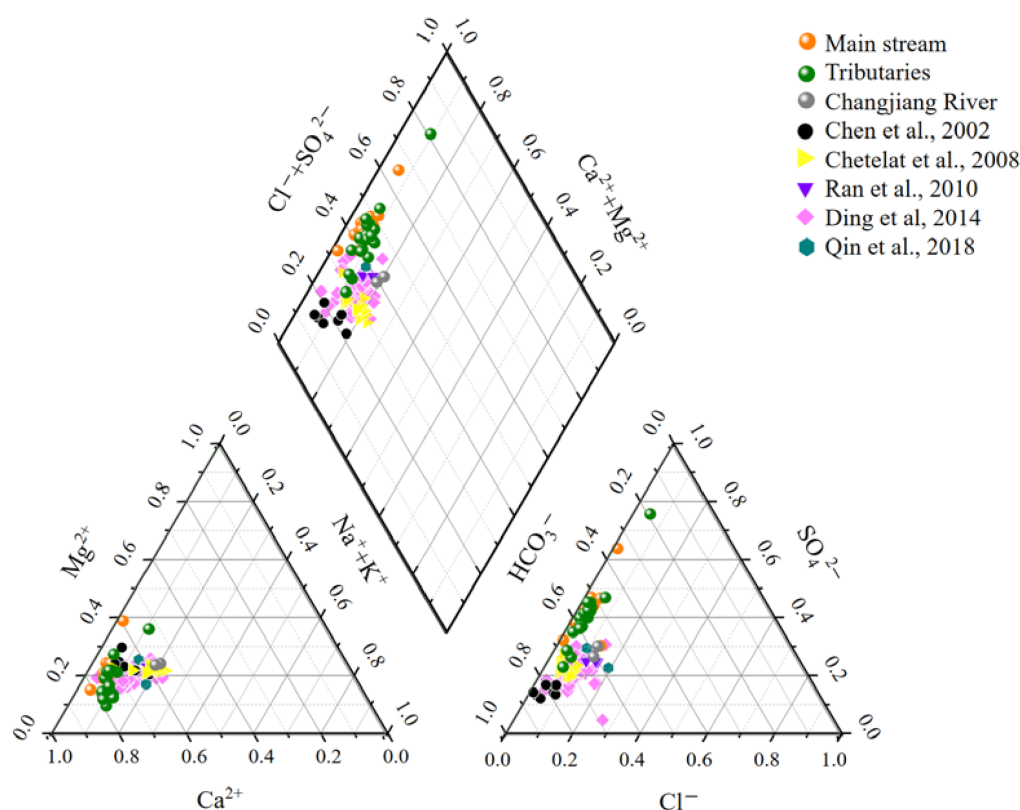
	Unit	Min	Max	Mean	SD	Chinese Guideline <sup>b</sup>	WHO Guideline <sup>b</sup>
Whole basin							
pH		7.63	8.87	8.35	0.27	6.5–8.5	6.5–8.5
EC	$\mu\text{S}/\text{cm}$	128	738	403	117	—	—
T	$^{\circ}\text{C}$	8.6	14.7	10.8	1.4	—	—
DO	mg/L	0.40	9.38	8.18	1.52	—	—
$\text{Na}^+$	mmol/L	0.06	0.78	0.30	0.17	—	—
$\text{K}^+$	mmol/L	0.02	0.19	0.05	0.03	—	—
$\text{Mg}^{2+}$	mmol/L	0.08	1.56	0.48	0.26	—	—
$\text{Ca}^{2+}$	mmol/L	0.44	2.79	1.54	0.46	—	—
$\text{F}^-$	mmol/L	0.00	0.02	0.01	0.00	0.05	0.08
$\text{Cl}^-$	mmol/L	0.04	0.55	0.18	0.14	7.05	7.05
$\text{NO}_3^-$	mmol/L	0.002	0.750	0.193	0.130	1.428	3.570
$\text{SO}_4^{2-}$	mmol/L	0.20	2.64	0.85	0.41	2.60	2.60
$\text{HCO}_3^-$	mmol/L	0.52	5.49	2.22	0.79	—	—
$\text{NH}_4^{+a}$	mmol/L	0.000	0.010	0.003	—	0.036	0.107
$\delta^{34}\text{S}-\text{SO}_4^{2-}$	‰	−7.79	22.13	4.68	6.21	—	—
SAR		0.04	0.61	0.21	0.11	—	—
Na%		1.27	19.02	6.98	3.41	—	—
RSC		−5.26	−0.49	−1.81	0.88	—	—
Main stream							
pH		7.63	8.87	8.36	0.28		
EC	$\mu\text{S}/\text{cm}$	381	480	428	32		
T	$^{\circ}\text{C}$	9.5	14.7	11.0	1.4		
DO	mg/L	6.85	9.35	8.34	0.67		
$\text{Na}^+$	mmol/L	0.06	0.78	0.30	0.18		
$\text{K}^+$	mmol/L	0.03	0.07	0.05	0.01		
$\text{Mg}^{2+}$	mmol/L	0.34	0.90	0.52	0.13		
$\text{Ca}^{2+}$	mmol/L	1.13	1.96	1.62	0.23		
$\text{F}^-$	mmol/L	0.00	0.01	0.01	0.00		
$\text{Cl}^-$	mmol/L	0.05	0.55	0.19	0.15		
$\text{NO}_3^-$	mmol/L	0.002	0.750	0.207	0.156		
$\text{SO}_4^{2-}$	mmol/L	0.54	1.35	0.89	0.19		
$\text{HCO}_3^-$	mmol/L	1.47	3.09	2.38	0.38		
$\delta^{34}\text{S}-\text{SO}_4^{2-}$	‰	−7.79	14	2.84	5.36		
SAR		0.04	0.61	0.21	0.14		
Na%		1.27	19.02	6.53	4.31		
RSC		−2.94	−0.79	−1.92	0.48		

Table 1. Cont.

	Unit	Min	Max	Mean	SD	Chinese Guideline <sup>b</sup>	WHO Guideline <sup>b</sup>
Tributaries							
pH		7.75	8.75	8.34	0.27		
EC	μS/cm	128	738	379	160		
T	°C	8.6	13.1	10.5	1.3		
DO	mg/L	0.40	9.38	8.03	2.04		
Na <sup>+</sup>	mmol/L	0.12	0.75	0.29	0.16		
K <sup>+</sup>	mmol/L	0.02	0.19	0.05	0.04		
Mg <sup>2+</sup>	mmol/L	0.08	1.56	0.42	0.35		
Ca <sup>2+</sup>	mmol/L	0.44	2.79	1.44	0.61		
F <sup>-</sup>	mmol/L	0.00	0.02	0.01	0.00		
Cl <sup>-</sup>	mmol/L	0.04	0.53	0.17	0.13		
NO <sub>3</sub> <sup>-</sup>	mmol/L	0.017	0.422	0.178	0.094		
SO <sub>4</sub> <sup>2-</sup>	mmol/L	0.20	2.64	0.82	0.57		
HCO <sub>3</sub> <sup>-</sup>	mmol/L	0.52	5.49	2.04	1.07		
δ <sup>34</sup> S-SO <sub>4</sub> <sup>2-</sup>	‰	-6.33	22.13	6.51	6.59		
SAR		0.11	0.39	0.21	0.07		
Na%		4.08	10.77	7.48	2.02		
RSC		-5.26	-0.49	-1.68	1.18		

Note: <sup>a</sup> the data of concentration is from [23]; <sup>b</sup> the unit of related values in Chinese guideline and WHO guideline are converted to mmol/L.

The major chemical ions of the Chishui River water are presented in Figure 2. It is very distinct that the principal cation in Chishui River is Ca<sup>2+</sup>, which accounts for 71 ± 6% (mean ± SD) of the cations, followed by Mg<sup>2+</sup> (21 ± 6%) and Na<sup>+</sup> + K<sup>+</sup> (8 ± 3%). The anions sequence is HCO<sub>3</sub><sup>-</sup> (55 ± 9%) > SO<sub>4</sub><sup>2-</sup> (41 ± 9%) > Cl<sup>-</sup> (4 ± 3%). HCO<sub>3</sub><sup>-</sup> is therefore the predominant anion in Chishui River, which is a widely confirmed product (as well as riverine Ca<sup>2+</sup> and Mg<sup>2+</sup>) of CO<sub>2</sub>-associated weathering process without the influence of anthropogenic pollution [13,24]. The massive carbonate sedimentary rock distribution in such a karst landscape river watershed creates the advantageous conditions for the chemical weathering of Ca/Mg-contented rock. Although the lower reaches flow through the area where the siliciclastic sedimentary rock developed, the inheritance of river water will make the lower reach reveal the characteristics of dissolved loads from upper and middle streams. Generally, the weathering rate of carbonate rock is much higher than other rocks in the same situations [25,26], implying that the HCO<sub>3</sub><sup>-</sup>, Ca<sup>2+</sup>, and Mg<sup>2+</sup>, derived from carbonate sedimentary rock weathering and exported into Chishui River in upper-middle stream, are far more than the potential Na<sup>+</sup> and K<sup>+</sup> originated from the weathering of siliciclastic sedimentary rock in the lower stream. Therefore, the hydrochemical type of Chishui River water is a Ca-Mg-HCO<sub>3</sub><sup>-</sup> type controlled by carbonate weathering, which is highly in agreement with the studies of the whole Changjiang River (Yangtze River) basin (Figure 2).



**Figure 2.** Piper diagrams representing the percentages of hydrochemical species in Chishui River (including 2 water samples collected in Changjiang River before and after the Chishui River drained into, the solid gray circle) and Changjiang River (data reported by previous studies [10,27–30]).

The potential sources of riverine  $\text{SO}_4^{2-}$  mainly include weathering process, atmospheric precipitation, industrial/mining activities, and sewage inputs [10]. Chemical weathering related studies have found that the accelerated carbonate dissolution occurred with relatively high  $\text{SO}_4^{2-}$  concentrations (as an agency of weathering processes) in the karst region [31,32]. Thus, the considerable fraction of  $\text{SO}_4^{2-}$  ( $41 \pm 9\%$ , close to  $\text{HCO}_3^-$ ) is non-negligible.

### 3.2. Source of Fluvial Solutes

#### 3.2.1. Stoichiometry–Revealed Sources of Solutes

In hydrochemistry studies, the high  $\text{Cl}^-$  concentration could be applied as a significant index of anthropogenic inputs (mainly in urban area) and domestic sewage [33]. Generally, the river nitrate originated from agricultural synthetic fertilizers exhibits a high  $\text{NO}_3^-$  concentration and a high value of  $\text{NO}_3^-/\text{Cl}^-$  ratio, while the domestic sewage presents low  $\text{NO}_3^-/\text{Cl}^-$  ratio and high concentration of  $\text{Cl}^-$  due to highly organic matter [34]. As shown in Figure 3a, the high  $\text{NO}_3^-/\text{Cl}^-$  ratio and low level of  $\text{Cl}^-$  concentration (range 0.04–0.55 meq/L, mean value  $0.18 \pm 0.14$  meq/L) were observed in all water samples of Chishui River, suggesting the major contribution by agricultural input (fertilizer), which can be supported by the large distribution area of cropland (~19.6%) in the whole watershed [7]. By contrast, the potential  $\text{Cl}^-$  inputs from the anthropogenic domestic sewage in urban region may be assuaged by various landscape setting and the well-mixed processes of river water, further resulting in a low concentration of riverine  $\text{Cl}^-$ . Moreover, although previous work have revealed that rainwater  $\text{NO}_3^-$  could be a significant contributor (even up to 71%) of riverine  $\text{NO}_3^-$  during storm-frequency season [35], however, the river water  $\text{NO}_3^-$  concentration ( $0.19 \pm 0.13$  meq/L) in the study period (dry season) was much higher than the karst rainwater  $\text{NO}_3^-$  concentration (typically  $< 0.04$  meq/L) [36–38]. Therefore, the contribution of wet deposition to Chishui River water  $\text{NO}_3^-$  is very limited.

In addition, the river water  $\text{SO}_4^{2-}/\text{Ca}^{2+}$  ratios were much higher than the  $\text{NO}_3^-/\text{Ca}^{2+}$  ratios (Figure 3b), indicating an additional potential impact of industrial activities and mining (e.g., pyrite in middle reaches) on fluvial solutes [39,40].

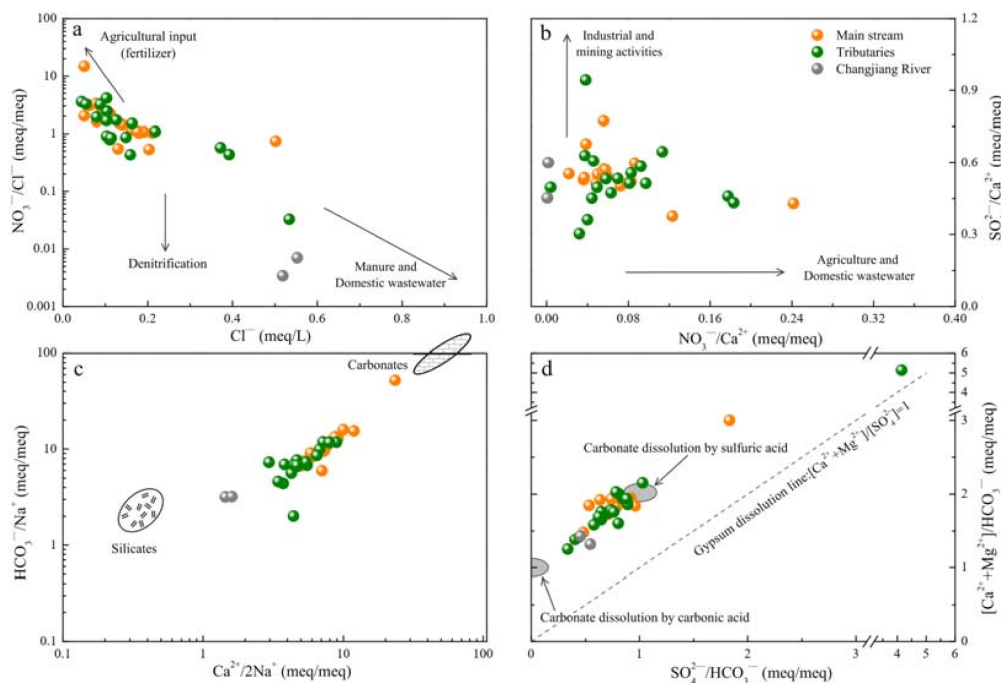


**Figure 3.** The relationship between  $\text{Cl}^-$  and  $\text{NO}_3^-/\text{Cl}^-$  ratios (a),  $\text{NO}_3^-/\text{Ca}^{2+}$  ratios and  $\text{SO}_4^{2-}/\text{Ca}^{2+}$  ratios (b),  $\text{Ca}^{2+}/2\text{Na}^+$  ratios and  $\text{HCO}_3^-/\text{Na}^+$  ratios (c),  $[\text{Ca}^{2+} + \text{Mg}^{2+}]/\text{HCO}_3^-$  ratios and  $\text{SO}_4^{2-}/\text{HCO}_3^-$  ratios (d) in Chishui River watershed.

The weathering-derived major ions always present typical ratios, thus the ratios of  $\text{Ca}^{2+}/\text{Na}^+$  and  $\text{HCO}_3^-/\text{Na}^+$  are the useful index to track the weathering origins of ions [13,19]. The  $\text{Ca}^{2+}/\text{Na}^+$  and  $\text{HCO}_3^-/\text{Na}^+$  ratios of Chishui River water were scattered between the silicate and carbonate end-members and more inclined to the carbonate source (Figure 3c), implying the leading role of carbonate weathering products on riverine ions with a slightly mixing process of silicate weathering products. It is noteworthy that the two samples from Changjiang River were more trended to silicate end-members (Figure 3c), indicating the differentiated weathering contributions of various rocks in upper Changjiang River.

According to the chemical reaction equation between carbonate minerals ( $\text{Ca}_x\text{Mg}_{(1-x)}\text{CO}_3$ ) and  $\text{H}_2\text{SO}_4$  or  $\text{H}_2\text{CO}_3$  ( $\text{H}_2\text{O} + \text{CO}_2$ ), the relationships between the  $[\text{Ca}^{2+} + \text{Mg}^{2+}]/\text{HCO}_3^-$  ratios and  $\text{SO}_4^{2-}/\text{HCO}_3^-$  ratios could reveal specific weathering process. If the  $\text{Ca}_x\text{Mg}_{(1-x)}\text{CO}_3$  are only weathered by  $\text{H}_2\text{CO}_3$ , the  $\text{SO}_4^{2-}/\text{HCO}_3^-$  should be  $\sim 0$  and the  $[\text{Ca}^{2+} + \text{Mg}^{2+}]/\text{HCO}_3^-$  ratio should be  $\sim 1$ . However, when only sulfuric acid is involved in chemical weathering of carbonate minerals, the  $\text{SO}_4^{2-}/\text{HCO}_3^- \approx 1$  and  $[\text{Ca}^{2+} + \text{Mg}^{2+}]/\text{HCO}_3^- \approx 2$ . In Figure 3d, most of samples distributed between the two types of acid-involved weathering results, implying that both  $\text{H}_2\text{SO}_4$  and  $\text{H}_2\text{CO}_3$  weathering processes occurred. The samples were relatively closer to the  $\text{H}_2\text{SO}_4$ -involved weathering results, indicating the importance of sulfuric acid weathering processes, which may notably accelerate the rock dissolution. The generally low  $\text{Mg}^{2+}/\text{Ca}^{2+}$  ratios ( $< 0.5$ ) of most river water samples further distinguished the contributions of different types of carbonate minerals, that is, the riverine  $\text{Ca}^{2+}$  and  $\text{Mg}^{2+}$  were primarily controlled by calcite dissolution (the dolomite dissolution dominated river water  $\text{Mg}^{2+}/\text{Ca}^{2+} \approx 1$ ) [26]. In contrast, if the extensive silicate weathering occurs, the  $[\text{Ca}^{2+} + \text{Mg}^{2+}]/\text{HCO}_3^-$  ratios will decrease and the sample points in Figure 3d will move downwards systematically due to the simultaneously production of  $\text{Na}^+$ ,  $\text{K}^+$ ,  $\text{HCO}_3^-$ , and  $\text{SO}_4^{2-}$  in silicate weathering [11,41].

However, there were no samples with  $[\text{Ca}^{2+} + \text{Mg}^{2+}]/\text{HCO}_3^- < 1$  found in Chishui River, further reflecting the negligibility of silicate weathering contribution. In addition, all samples were completely above the gypsum dissolution line ( $[\text{Ca}^{2+} + \text{Mg}^{2+}]/\text{SO}_4^{2-} = 1$ ) (Figure 3d), demonstrating the limited contribution of gypsum dissolution to riverine solutes [19,42]. Similar to  $\text{H}_2\text{SO}_4$ , the nitric acid ( $\text{HNO}_3$ ) could also accelerate the weathering processes via dissolving the minerals [1], particularly in a small karst watershed scale with high nitrate loads [15,17,18]. Given the  $\text{NO}_3^-$  concentration much lower than  $\text{HCO}_3^-$  and  $\text{SO}_4^{2-}$  concentration (Table 1), here we concluded that the  $\text{HNO}_3$ -related rock weathering was also relatively limited.

According to low concentrations of riverine  $\text{K}^+$  (0.05 mmol/L),  $\text{F}^-$  (0.01 mmol/L), and  $\text{NH}_4^+$  (0.003 mmol/L) [23], these three ions related ratios were not presented in Figure 3. Even so, previous studies have concluded that  $\text{K}^+$  is contributed both by rock weathering (silicate) and human emissions [10,41,43]. Thus, here we hold the opinion that  $\text{K}^+$  is mainly controlled by rock source in such a low riverine  $\text{K}^+$  level (anthropogenic input is negligible) in Chishui River. Riverine  $\text{F}^-$  is also primarily originated from bedrocks [44]. As for  $\text{NH}_4^+$ , the agriculture-related processes, mainly ammonia-contained fertilizer, can be an interpretation for the samples with relatively high ammonia concentration [45].

### 3.2.2. PCA Analysis

The PCA was used to further explore the potential sources of riverine ions in Chishui River. Three principal components (PCs) with eigenvalues exceeding 1 were distinguished and illustrated in Figure 4, with more details presented in Table 2. These three PCs contained a total of 79.67% variance. The PC 1, PC 2, and PC 3 accounted for 33.8%, 23.9%, and 23.1% of total variances, respectively. Four ions ( $\text{K}^+$ ,  $\text{Mg}^{2+}$ ,  $\text{F}^-$ , and  $\text{HCO}_3^-$ ) as well as EC presented notably positive loadings in PC 1, and the relatively strong loading of  $\text{Ca}^{2+}$  (0.48) is also found in PC 1 (Figure 4 and Table 2). Based on the stoichiometry discussed in Section 3.2.1, here we infer that PC 1 was mainly contributed by natural rock weathering inputs in the Chishui River watershed due to the high loadings of feature ions of rock weathering (primarily carbonate) [46].  $\text{Na}^+$  and  $\text{Cl}^-$  presented clear positive loadings in PC 2, but these two ions were weakly loaded in PC 1 (natural source) and PC 3 ( $\text{SO}_4^{2-}$ -dominated human inputs). Combined with the negligible contribution of silicate weathering and the limited anthropogenic  $\text{Cl}^-$  inputs mentioned before, the atmospheric input/deposition could be a reasonable contributor, which is also supported by previous studies [42]. The strongest loadings of  $\text{SO}_4^{2-}$  and  $\text{NO}_3^-$  were observed in PC 3 (Figure 4), considering as typical anthropogenic inputs. It is noteworthy that the PC 3 also presented a significantly positive loading of  $\text{Ca}^{2+}$ , further supporting the  $\text{H}_2\text{SO}_4$ -involved weathering processes. Additionally, the same positive loading of EC (reflect total riverine ion content) was found in PC 1 and PC 3 (Table 2), indicating that the contribution of natural and anthropogenic sources to total fluvial ions was comparable.

### 3.3. Sulfur Isotope-Based Source Identification of Riverine Sulfate

Although limited impact of fluvial  $\text{SO}_4^{2-}$  for drinking and irrigation purpose is reported, the potential accelerated weathering may result in more solutes input to river system, which further causes other environmental issues (e.g., carbon source/sink variations) [11]. Therefore, to further constrain the  $\text{SO}_4^{2-}$  sources, the effective indicator  $\delta^{34}\text{S}\text{-SO}_4^{2-}$  was applied. Generally, the riverine  $\text{SO}_4^{2-}$  is derived from four sources: atmospheric inputs (mainly rainwater); sulfide oxidation (e.g., pyrite); human inputs (e.g., agricultural fertilizers, sewage, and industrial effluent); gypsum dissolution (a kind of evaporitic rock) [12,14,47]. These four sources can be well constrained by combining the distinguished  $\delta^{34}\text{S}\text{-SO}_4^{2-}$  values and  $\text{SO}_4^{2-}$  concentrations (Figure 5).

The sulfur isotope compositions of atmospheric depositions in south China were well explored in previous studies, such as the 950-day based study in Wuhan urban area ( $\delta^{34}\text{S}\text{-SO}_4^{2-} = +4.5 \pm 1.3\text{‰}$ ) [48], rainwater in Sichuan Basin ( $\delta^{34}\text{S}\text{-SO}_4^{2-} = +1.5 \sim +6.0\text{‰}$ ) [49], and the rainwater sulfur isotope study carried out in a karst agricultural

catchment ( $\delta^{34}\text{S}\text{-SO}_4^{2-} = +1.3 \pm 6.2\%$ ) [50]. Based on the similar geographical location, climatic condition, lithology and agriculture-dominated industrial structure, the rainwater  $\delta^{34}\text{S}\text{-SO}_4^{2-}$  values ( $+1.3 \pm 6.2\%$ ) of the karst agricultural catchment can be regarded as an atmospheric input end-member. The sulfide oxidation derived  $\text{SO}_4^{2-}$  usually inherit the sulfur isotope compositions of the initial sulfide due to limited isotope fractionation during oxidation processes [19]. The average  $\delta^{34}\text{S}\text{-SO}_4^{2-}$  value of pyrites in the study area (Sichuan, Guizhou, and Yunnan provinces) was  $-7.8\%$  [51], which is within the typical range of sulfide ( $-13.0\sim-1.1\%$ ) [19]. Moreover, although the sulfide oxidated  $\text{SO}_4^{2-}$  concentrations were rarely reported in the study area, previous work have shown that its concentration should be exceed 0.1 mol/L [47], even up to 2 mol/L, that is,  $1/[\text{SO}_4^{2-}] = 0.5\sim 10$ . The anthropogenic inputs, mainly including agricultural fertilizers, domestic and industrial sewage, present a wide range of sulfur isotope compositions. Therefore, the typical  $\delta^{34}\text{S}\text{-SO}_4^{2-}$  values of water in farmland and livestock farm areas ( $+2.8\sim+13.9\%$ ) were regarded as the end-member of human inputs [12,52], and the potentially high  $\text{SO}_4^{2-}$  concentration ( $1/[\text{SO}_4^{2-}]$  below  $\sim 17.5$ ) [19] was selected to distinguish the overlapped part of the  $\delta^{34}\text{S}\text{-SO}_4^{2-}$  values with atmospheric input. Moreover, the gypsum dissolution source presented the highest  $\delta^{34}\text{S}\text{-SO}_4^{2-}$  value (up to  $\sim+30\%$ ) [2] and high  $\text{SO}_4^{2-}$  concentration.

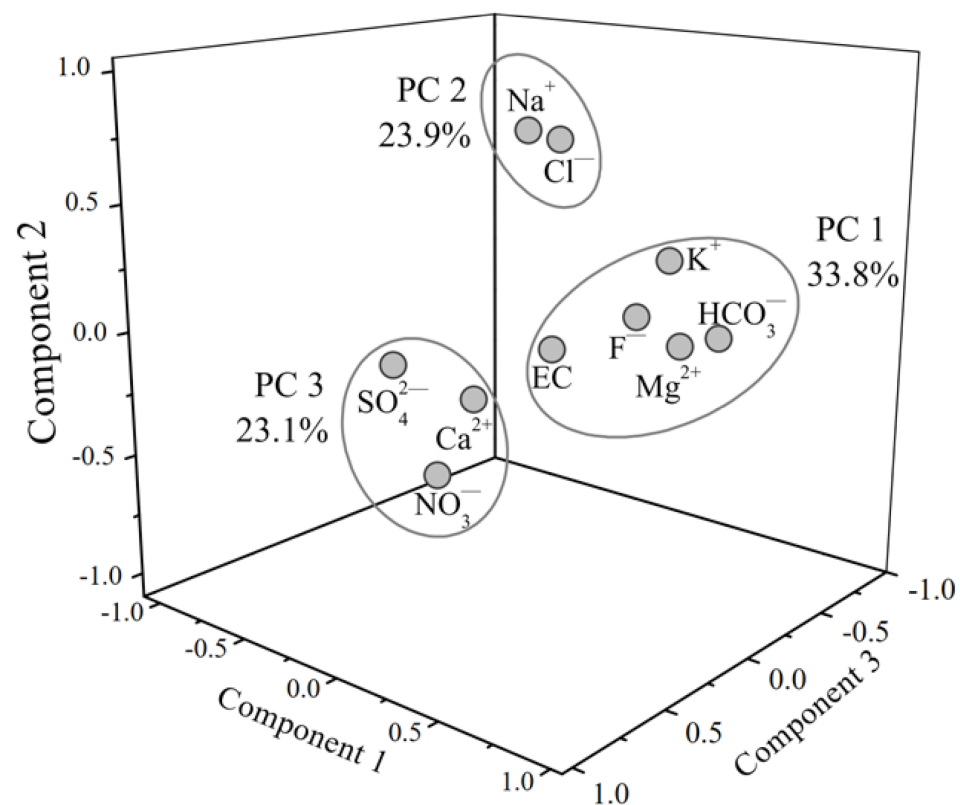


**Figure 4.** The 3D plot of factor loadings of Chishui River ions and other parameters.

As shown in Figure 5, the ternary diagram presented the relative contributions of different origins to fluvial  $\text{SO}_4^{2-}$  via the relationship between  $\delta^{34}\text{S}\text{-SO}_4^{2-}$  values and  $1/[\text{SO}_4^{2-}]$ , this is, riverine  $\text{SO}_4^{2-}$  were controlled by the sources of human inputs and sulfide oxidation. The middle-stream-distributed pyrite deposits and the relatively high population density (282 persons per  $\text{km}^2$ ) and wide urbanization area (1.2%) [7,23,40] also underpinned these results. It is noteworthy that four samples were distributed over the range of human inputs and tended into the gypsum dissolution sources (Figure 5). This suggests the potential influence of gypsum dissolution on river water in some sampling sites to a certain extent, but it was negligible on a whole watershed scale, which was also

supported by previous work [19]. Although the range of  $\delta^{34}\text{S-SO}_4^{2-}$  value of atmospheric inputs was partially overlapped with other sources, the much lower  $\text{SO}_4^{2-}$  concentrations of atmospheric source were significantly separated from human input and sulfide oxidation sources (Figure 5), confirming again that the contribution of atmospheric inputs to riverine sulfate was very limited. This can also be supported by the average investigation results of global rivers (atmospheric input contributed to  $\sim 3\%$  sulfate) [13]. In comparison, the water samples obtained in larger-scale Zhujiang River watershed (originated in karst region of Guizhou province) in Figure 5 presented a distribution closer to the sulfide oxidation end-member, with some samples trended to the atmospheric source [11], indicating a complicated mixing processes and differential contributions of sulfate sources in different scaled catchments.

**Table 2.** Varimax rotated component matrix for water ions in Chishui River.

Eigenvalues	5.78	2.03	1.07	Communalities
Variance (%)	33.80	23.90	23.10	
Cumulative (%)	33.80	57.70	80.80	
Variable	PC 1	PC 2	PC 3	
EC	0.69	0.19	0.69	0.97
Na <sup>+</sup>	0.27	0.84	0.33	0.88
K <sup>+</sup>	0.75	0.40	0.14	0.75
Mg <sup>2+</sup>	0.91	0.14	0.28	0.92
Ca <sup>2+</sup>	0.48	0.01	0.85	0.95
F <sup>-</sup>	0.70	0.21	0.26	0.61
Cl <sup>-</sup>	0.33	0.80	0.24	0.81
NO <sub>3</sub> <sup>-</sup>	-0.13	-0.54	0.40	0.47
SO <sub>4</sub> <sup>2-</sup>	0.19	0.09	0.92	0.90
HCO <sub>3</sub> <sup>-</sup>	0.94	0.14	0.10	0.92

Note: Extraction method: Principal component analysis; Rotation method: Varimax with Kaiser normalization; The significance of KMO and Bartlett's sphericity test is  $<0.001$ .

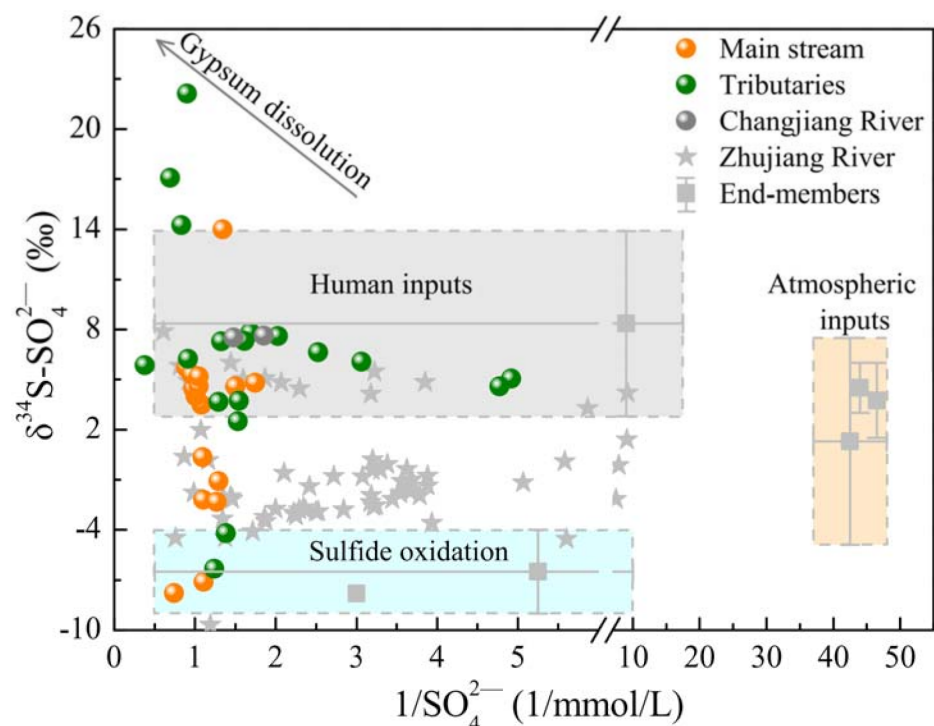


**Figure 5.** The relationship between  $\delta^{34}\text{S-SO}_4^{2-}$  values and  $\text{SO}_4^{2-}$  concentrations revealing the mixing processes of riverine sulfate from different sources. The data of Zhujiang River is from [11].

### 3.4. Water Quality and Risk Assessment

#### 3.4.1. Irrigation and Guideline-Based Water Quality

Chishui River servers as primary water resources of the agriculture, industry, and local residents (population > 5 million). As summarized in Table 1, according to the Chinese and WHO drinking water quality guidelines, the desirable pH value for drinking is recommended between 6.5~8.5, thus most of the water samples (81.6%) had suitable pH values (Table S1). The high pH values (>8.5) of partial samples were mainly caused by carbonate weathering. Most of the guidelines-covered ions, including  $F^-$ ,  $Cl^-$ ,  $NO_3^-$ , and  $NH_4^+$  of all river water samples were below the recommended limits. However, although the average value of riverine  $SO_4^{2-}$  (0.85 mmol/L) was lower than that of guidelines limits (2.60 mmol/L), the maximum value of riverine  $SO_4^{2-}$  (2.64 mmol/L) exceeded the permissible limits, which needs more attention. The previous study on trace metal also assessed the 19 metals-based water quality index (WQI) of Chishui River, which showed the assessment results of excellent water quality (WQI < 50, only from the perspective of metals) without extensive trace metal contamination [7].

The Na% and SAR indicators can reflect the Na hazard to agricultural land by irrigation-influenced soil aggregate [19]. According to the calculated SAR and Na% values, all water samples in the Chishui River could be regarded as excellent/good quality (SAR < 0.61; Na% < 19.0%) with no samples out of the desirable limits (SAR = 1; Na% = 30.0%). For the residual sodium carbonate (RSC), there was no water samples present a RSC value exceeded 1.25 (Table S1), indicating the well suitability of irrigation water. Moreover, the United States Salinity Laboratory (USSL) diagram and Wilcox diagram were plotted based on the EC, SAR, and Na% values (Figure 6), and all the Chishui River water samples were scattered in the C1S1 and C2S1 zone of USSL diagram and the ‘Excellent to Good’ area of Wilcox diagram. Overall, the Chishui River water is desirable for agricultural irrigation and will not bring about the soil hazard. However, the continuous long-term monitoring is still a worthy mission due to the enhanced human activities.

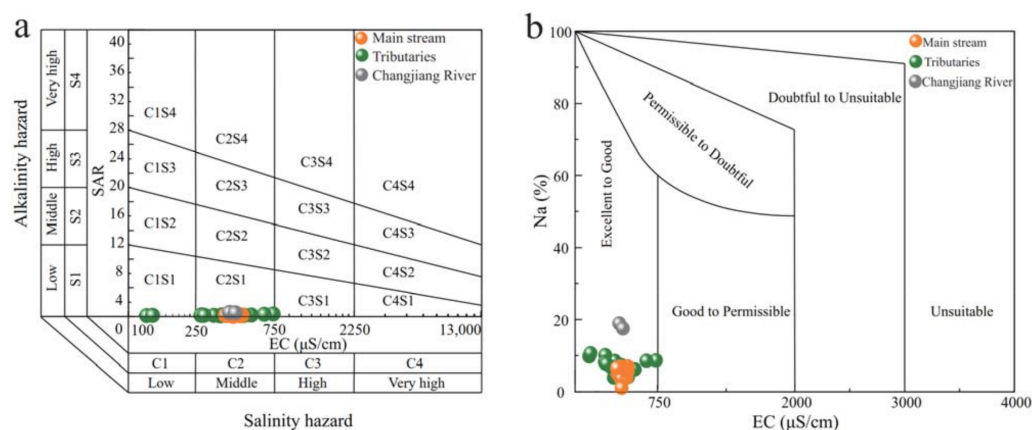


**Figure 6.** Irrigation water quality assessment alkalinity and salinity: (a) United States Salinity Laboratory (USSL) diagram and (b) Wilcox diagram.

#### 3.4.2. Health Risk Assessment

Among the major ions in natural water, excessive exposure (ingestion intake) of  $F^-$ ,  $NO_3^-$ , and  $NH_4^+$  can cause typical non-carcinogenic hazards, while  $SO_4^{2-}$  does not result in health issue [11]. Thus, riverine  $F^-$ ,  $NO_3^-$ , and  $NH_4^+$  were involved in the health risk assessment in this study. The average concentration-based HQ values were calculated and presented in Figure 7. The HQ values of three assessed ions were in the order of  $HQ-NO_3^-$  ( $0.28 \pm 0.19$ ) >  $HQ-F^-$  ( $0.13 \pm 0.06$ ) >  $HQ-NH_4^+$  ( $0.002 \pm 0.000$ ) for children and  $HQ-NO_3^-$  ( $0.11 \pm 0.07$ ) >  $HQ-F^-$  ( $0.05 \pm 0.02$ ) >  $HQ-NH_4^+$  ( $0.001 \pm 0.000$ ) for adult. The results were similar to other researches [44], that is,  $NH_4^+$  occupied a tiny part of the total HQ, while  $NO_3^-$  and  $F^-$  were the majority. For both children and adults, HQs of each

ion and total HQ were all lower than the hazard level ( $<1$ ), indicating a lower health risk of assessed ions. It is noteworthy that the HQ value for children was always higher than that for adults, implying that children were facing higher risks from riverine ions compared to adults. In addition, the potential harmful health effects can also occur if the HQ value is greater than 0.1 for children [21]. Therefore, the riverine ion-related health risk is not completely negligible, particularly for children.

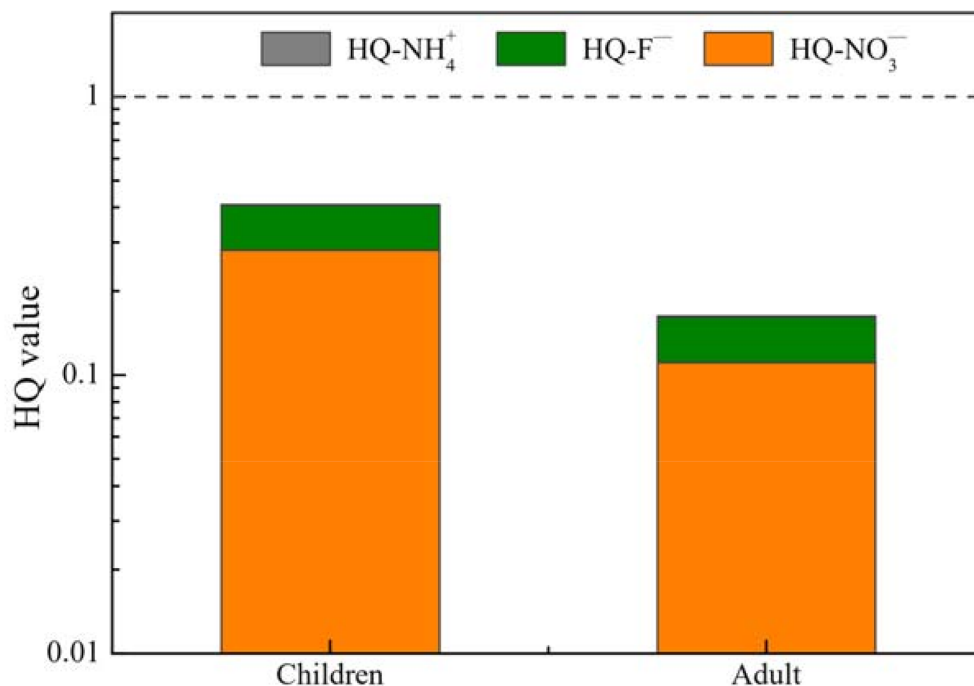


Figure 7. Non-carcinogenic health risk assessment of fluorine, nitrate, ammonia in Chishui River water.

#### 4. Conclusions

The present study aimed to investigate hydrochemical compositions and sulfur isotope compositions of Chishui River water, southwest of China. Based on the isotope tracer, stoichiometry and PCA method, the sources of major ions were identified. The rock (mainly carbonate) weathering inputs were the primary sources of  $\text{K}^+$ ,  $\text{Mg}^{2+}$ ,  $\text{Ca}^{2+}$ ,  $\text{F}^-$ ,  $\text{HCO}_3^-$ , and atmospheric contribution was the source of  $\text{Na}^+$  and  $\text{Cl}^-$ , while the anthropogenic input was responsible for  $\text{SO}_4^{2-}$  and  $\text{NO}_3^-$ . Sulfur isotope compositions further reflected the relative contribution of different sources, that is, the contribution of human inputs (main) and sulfide oxidation controlled the riverine  $\text{SO}_4^{2-}$ , but the input of atmospheric deposition was limited. Both the water quality and hazard quotient assessment produced good results, indicating the suitable aims of river water for drinking and irrigation. This work and the possible continuing study would be benefit to the prevention of watershed water environment and further help planning the sustainable water resources in Chishui River watershed.

**Supplementary Materials:** The following are available online at <https://www.mdpi.com/article/10.3390/w13091231/s1>, Table S1: The water parameters, major ion compositions,  $\delta^{34}\text{S}-\text{SO}_4^{2-}$  values, SAR, Na%, RSC,  $[\text{TZ}^+ - \text{TZ}^-]/\text{TZ}^-$  of Chishui River.

**Author Contributions:** Conceptualization, Q.W. and X.G.; methodology, Q.W. and X.G.; software, X.G.; validation, Q.W.; formal analysis, X.G., Q.W., Z.W., S.G. and T.W.; investigation, Q.W.; resources, Q.W. and Z.W.; writing—original draft preparation, X.G. and Q.W.; writing—review and editing, X.G., Q.W. and Z.W.; supervision, Q.W.; project administration, Q.W. and Z.W.; funding acquisition, Q.W. and Z.W. All authors have read and agreed to the published version of the manuscript.

**Funding:** This research was funded by the Joint Fund of the National Natural Science Foundation of China and Guizhou Province, China (U1612442), the National Natural Science Foundation of China (41863004, 41863003, 41763019), the first-class discipline construction project in Guizhou Province–Public Health and Preventive Medicine (No. 2017[85], GNYL [2017]007), and the Guizhou Science and Technology Support Program ([2019]2832). The funders had no role in study design, data collection and analysis, decision to publish, or preparation of the manuscript.

**Institutional Review Board Statement:** Not applicable.

**Informed Consent Statement:** Not applicable.

**Data Availability Statement:** The data are presented in this study are available in Supplementary Materials.

**Conflicts of Interest:** The authors declare no conflict of interest.

## References

- Barnes, R.T.; Raymond, P.A. The contribution of agricultural and urban activities to inorganic carbon fluxes within temperate watersheds. *Chem. Geol.* **2009**, *266*, 318–327. [\[CrossRef\]](#)
- Nightingale, M.; Mayer, B. Identifying sources and processes controlling the sulphur cycle in the Canyon Creek watershed, Alberta, Canada. *Isot. Environ. Health Stud.* **2012**, *48*, 89–104. [\[CrossRef\]](#)
- Zeng, J.; Han, G. Preliminary copper isotope study on particulate matter in Zhujiang River, southwest China: Application for source identification. *Ecotoxicol. Environ. Saf.* **2020**, *198*, 110663. [\[CrossRef\]](#) [\[PubMed\]](#)
- Wang, J.; Jiang, Y.; Sun, J.; She, J.; Yin, M.; Fang, F.; Xiao, T.; Song, G.; Liu, J. Geochemical transfer of cadmium in river sediments near a lead-zinc smelter. *Ecotoxicol. Environ. Saf.* **2020**, *196*, 110529. [\[CrossRef\]](#) [\[PubMed\]](#)
- Zaric, N.M.; Deljanin, I.; Ilijević, K.; Stanisavljević, L.; Ristić, M.; Gržetić, I. Assessment of spatial and temporal variations in trace element concentrations using honeybees (*Apis mellifera*) as bioindicators. *PeerJ* **2018**, *6*, e5197. [\[CrossRef\]](#) [\[PubMed\]](#)
- Wang, J.; Wang, L.; Wang, Y.; Tsang, D.C.W.; Yang, X.; Beiyuan, J.; Yin, M.; Xiao, T.; Jiang, Y.; Lin, W.; et al. Emerging risks of toxic metal(loid)s in soil-vegetables influenced by steel-making activities and isotopic source apportionment. *Environ. Int.* **2021**, *146*, 106207. [\[CrossRef\]](#)
- Xu, S.; Lang, Y.; Zhong, J.; Xiao, M.; Ding, H. Coupled controls of climate, lithology and land use on dissolved trace elements in a karst river system. *J. Hydrol.* **2020**, *591*, 125328. [\[CrossRef\]](#)
- Liu, M.; Han, G.; Zhang, Q. Effects of agricultural abandonment on soil aggregation, soil organic carbon storage and stabilization: Results from observation in a small karst catchment, Southwest China. *Agric. Ecosyst. Environ.* **2020**, *288*, 106719. [\[CrossRef\]](#)
- Chen, L.; Liu, J.-r.; Hu, W.-f.; Gao, J.; Yang, J.-y. Vanadium in soil-plant system: Source, fate, toxicity, and bioremediation. *J. Hazard. Mater.* **2021**, *405*, 124200. [\[CrossRef\]](#)
- Chetelat, B.; Liu, C.Q.; Zhao, Z.Q.; Wang, Q.L.; Li, S.L.; Li, J.; Wang, B.L. Geochemistry of the dissolved load of the Changjiang Basin rivers: Anthropogenic impacts and chemical weathering. *Geochim. Cosmochim. Acta* **2008**, *72*, 4254–4277. [\[CrossRef\]](#)
- Liu, J.; Han, G. Distributions and Source Identification of the Major Ions in Zhujiang River, Southwest China: Examining the Relationships Between Human Perturbations, Chemical Weathering, Water Quality and Health Risk. *Exposure Health* **2020**, *12*, 849–862. [\[CrossRef\]](#)
- Szynkiewicz, A.; Witcher, J.C.; Modelska, M.; Borrok, D.M.; Pratt, L.M. Anthropogenic sulfate loads in the Rio Grande, New Mexico (USA). *Chem. Geol.* **2011**, *283*, 194–209. [\[CrossRef\]](#)
- Gaillardet, J.; Dupré, B.; Louvat, P.; Allègre, C.J. Global silicate weathering and CO<sub>2</sub> consumption rates deduced from the chemistry of large rivers. *Chem. Geol.* **1999**, *159*, 3–30. [\[CrossRef\]](#)
- Xu, S.; Li, S.; Su, J.; Yue, F.; Zhong, J.; Chen, S. Oxidation of pyrite and reducing nitrogen fertilizer enhanced the carbon cycle by driving terrestrial chemical weathering. *Sci. Total Environ.* **2021**, *768*, 144343. [\[CrossRef\]](#)
- Zeng, J.; Yue, F.-J.; Wang, Z.-J.; Wu, Q.; Qin, C.-Q.; Li, S.-L. Quantifying depression trapping effect on rainwater chemical composition during the rainy season in karst agricultural area, southwestern China. *Atmos. Environ.* **2019**, *218*, 116998. [\[CrossRef\]](#)
- Han, G.; Tang, Y.; Liu, M.; Van Zwieten, L.; Yang, X.; Yu, C.; Wang, H.; Song, Z. Carbon-nitrogen isotope coupling of soil organic matter in a karst region under land use change, Southwest China. *Agric. Ecosyst. Environ.* **2020**, *301*, 107027. [\[CrossRef\]](#)
- Wang, Z.-J.; Li, S.-L.; Yue, F.-J.; Qin, C.-Q.; Buckerfield, S.; Zeng, J. Rainfall driven nitrate transport in agricultural karst surface river system: Insight from high resolution hydrochemistry and nitrate isotopes. *Agric. Ecosyst. Environ.* **2020**, *291*, 106787. [\[CrossRef\]](#)
- Yue, F.-J.; Waldron, S.; Li, S.-L.; Wang, Z.-J.; Zeng, J.; Xu, S.; Zhang, Z.-C.; Oliver, D.M. Land use interacts with changes in catchment hydrology to generate chronic nitrate pollution in karst waters and strong seasonality in excess nitrate export. *Sci. Total Environ.* **2019**, *696*, 134062. [\[CrossRef\]](#)
- Liu, J.; Han, G. Major ions and  $\delta^{34}\text{S}\text{SO}_4$  in Jiulongjiang River water: Investigating the relationships between natural chemical weathering and human perturbations. *Sci. Total Environ.* **2020**, *724*, 138208. [\[CrossRef\]](#)
- Cao, X.; Wu, P.; Zhou, S.; Sun, J.; Han, Z. Tracing the origin and geochemical processes of dissolved sulphate in a karst-dominated wetland catchment using stable isotope indicators. *J. Hydrol.* **2018**, *562*, 210–222. [\[CrossRef\]](#)

21. Zeng, J.; Han, G.; Yang, K. Assessment and sources of heavy metals in suspended particulate matter in a tropical catchment, northeast Thailand. *J. Clean. Prod.* **2020**, *265*, 121898. [[CrossRef](#)]
22. Gaillardet, J.; Dupre, B.; Allegre, C.J.; Négrel, P. Chemical and physical denudation in the Amazon River Basin. *Chem. Geol.* **1997**, *142*, 141–173. [[CrossRef](#)]
23. An, Y.; Jiang, H.; Wu, Q.; Yang, R.; Lang, X.; Luo, J. Assessment of water quality in the Chishui River Basin during low water period. *Resour. Environ. Yangtze Basin* **2014**, *23*, 1472–1478. (In Chinese)
24. Liu, J.; Han, G. Controlling factors of riverine CO<sub>2</sub> partial pressure and CO<sub>2</sub> outgassing in a large karst river under base flow condition. *J. Hydrol.* **2021**, *593*, 125638. [[CrossRef](#)]
25. Tipper, E.T.; Bickle, M.J.; Galy, A.; West, A.J.; Pomies, C.; Chapman, H.J. The short term climatic sensitivity of carbonate and silicate weathering fluxes: Insight from seasonal variations in river chemistry. *Geochim. Cosmochim. Acta* **2006**, *70*, 2737–2754. [[CrossRef](#)]
26. Zeng, J.; Yue, F.-J.; Li, S.-L.; Wang, Z.-J.; Wu, Q.; Qin, C.-Q.; Yan, Z.-L. Determining rainwater chemistry to reveal alkaline rain trend in Southwest China: Evidence from a frequent-rainy karst area with extensive agricultural production. *Environ. Pollut.* **2020**, *266*, 115166. [[CrossRef](#)] [[PubMed](#)]
27. Chen, J.; Wang, F.; Xia, X.; Zhang, L. Major element chemistry of the Changjiang (Yangtze River). *Chem. Geol.* **2002**, *187*, 231–255. [[CrossRef](#)]
28. Ran, X.; Yu, Z.; Yao, Q.; Chen, H.; Mi, T. Major ion geochemistry and nutrient behaviour in the mixing zone of the Changjiang (Yangtze) River and its tributaries in the Three Gorges Reservoir. *Hydrol. Process.* **2010**, *24*, 2481–2495. [[CrossRef](#)]
29. Tipping, D.; Gao, J.; Tian, S.; Shi, G.; Chen, F.; Wang, C.; Luo, X.; Han, D. Chemical and Isotopic Characteristics of the Water and Suspended Particulate Materials in the Yangtze River and Their Geological and Environmental Implications. *Acta Geol. Sin. Engl. Ed.* **2014**, *88*, 276–360. [[CrossRef](#)]
30. Qin, T.; Yang, P.; Groves, C.; Chen, F.; Xie, G.; Zhan, Z. Natural and anthropogenic factors affecting geochemistry of the Jialing and Yangtze Rivers in urban Chongqing, SW China. *Appl. Geochem.* **2018**, *98*, 448–458. [[CrossRef](#)]
31. Li, S.-L.; Calmels, D.; Han, G.; Gaillardet, J.; Liu, C.-Q. Sulfuric acid as an agent of carbonate weathering constrained by  $\delta^{13}\text{CDIC}$ : Examples from Southwest China. *Earth Planet. Sci. Lett.* **2008**, *270*, 189–199. [[CrossRef](#)]
32. Liu, J.; Han, G. Tracing Riverine Particulate Black Carbon Sources in Xijiang River Basin: Insight from Stable Isotopic Composition and Bayesian Mixing Model. *Water Res.* **2021**, *194*, 116932. [[CrossRef](#)]
33. Widory, D.; Petelet-Giraud, E.; Négrel, P.; Ladouche, B. Tracking the Sources of Nitrate in Groundwater Using Coupled Nitrogen and Boron Isotopes: A Synthesis. *Environ. Sci. Technol.* **2005**, *39*, 539–548. [[CrossRef](#)] [[PubMed](#)]
34. Yue, F.-J.; Li, S.-L.; Waldron, S.; Wang, Z.-J.; Oliver, D.M.; Chen, X.; Liu, C.-Q. Rainfall and conduit drainage combine to accelerate nitrate loss from a karst agroecosystem: Insights from stable isotope tracing and high-frequency nitrate sensing. *Water Res.* **2020**, *186*, 116388. [[CrossRef](#)]
35. Divers, M.T.; Elliott, E.M.; Bain, D.J. Constraining Nitrogen Inputs to Urban Streams from Leaking Sewers Using Inverse Modeling: Implications for Dissolved Inorganic Nitrogen (DIN) Retention in Urban Environments. *Environ. Sci. Technol.* **2013**, *47*, 1816–1823. [[CrossRef](#)] [[PubMed](#)]
36. Zeng, J.; Yue, F.-J.; Li, S.-L.; Wang, Z.-J.; Qin, C.-Q.; Wu, Q.-X.; Xu, S. Agriculture driven nitrogen wet deposition in a karst catchment in southwest China. *Agric. Ecosyst. Environ.* **2020**, *294*, 106883. [[CrossRef](#)]
37. Han, G.; Song, Z.; Tang, Y.; Wu, Q.; Wang, Z. Ca and Sr isotope compositions of rainwater from Guiyang city, Southwest China: Implication for the sources of atmospheric aerosols and their seasonal variations. *Atmos. Environ.* **2019**, *214*, 116854. [[CrossRef](#)]
38. Qu, R.; Han, G. A critical review of the variation in rainwater acidity in 24 Chinese cities during 1982–2018. *Elem. Sci. Anthr.* **2021**, *9*, 00142. [[CrossRef](#)]
39. Zuo, Y.; An, Y.; Wu, Q.; Qu, K.; Fan, G.; Ye, Z.; Qin, L.; Qian, J.; Tu, C. Study on the hydrochemical characteristics of Dulu River basin in Guizhou Province. *China Environ. Sci.* **2017**, *37*, 2684–2690. (In Chinese)
40. Luo, J.; An, Y.; Wu, Q.; Yang, R.; Jiang, H.; Peng, W.; Yu, X.; Lv, J. Spatial distribution of surface water chemical components in the middle and lower reaches of Chishui River Basin. *Earth Environ.* **2014**, *42*, 297–305. (In Chinese)
41. Xu, Z.; Liu, C.-Q. Chemical weathering in the upper reaches of Xijiang River draining the Yunnan–Guizhou Plateau, Southwest China. *Chem. Geol.* **2007**, *239*, 83–95. [[CrossRef](#)]
42. Han, G.; Liu, C.-Q. Water geochemistry controlled by carbonate dissolution: A study of the river waters draining karst-dominated terrain, Guizhou Province, China. *Chem. Geol.* **2004**, *204*, 1–21. [[CrossRef](#)]
43. Li, X.; Han, G.; Zhang, Q.; Miao, Z. An optimal separation method for high-precision K isotope analysis by using MC-ICP-MS with a dummy bucket. *J. Anal. At. Spectrom.* **2020**, *35*, 1330–1339. [[CrossRef](#)]
44. Li, P.; He, X.; Li, Y.; Xiang, G. Occurrence and Health Implication of Fluoride in Groundwater of Loess Aquifer in the Chinese Loess Plateau: A Case Study of Tongchuan, Northwest China. *Exposure Health* **2019**, *11*, 95–107. [[CrossRef](#)]
45. Xu, S.; Li, S.-L.; Zhong, J.; Li, C. Spatial scale effects of the variable relationships between landscape pattern and water quality: Example from an agricultural karst river basin, Southwestern China. *Agric. Ecosyst. Environ.* **2020**, *300*, 106999. [[CrossRef](#)]
46. Lee, K.-S.; Ryu, J.-S.; Ahn, K.-H.; Chang, H.-W.; Lee, D. Factors controlling carbon isotope ratios of dissolved inorganic carbon in two major tributaries of the Han River, Korea. *Hydrol. Process.* **2007**, *21*, 500–509. [[CrossRef](#)]
47. Han, G.; Tang, Y.; Wu, Q.; Liu, M.; Wang, Z. Assessing Contamination Sources by Using Sulfur and Oxygen Isotopes of Sulfate Ions in Xijiang River Basin, Southwest China. *J. Environ. Qual.* **2019**, *48*, 1507–1516. [[CrossRef](#)] [[PubMed](#)]

48. Li, X.; Bao, H.; Gan, Y.; Zhou, A.; Liu, Y. Multiple oxygen and sulfur isotope compositions of secondary atmospheric sulfate in a mega-city in central China. *Atmos. Environ.* **2013**, *81*, 591–599. [[CrossRef](#)]
49. Li, X.-D.; Masuda, H.; Kusakabe, M.; Yanagisawa, F.; Zeng, H.-A. Degradation of groundwater quality due to anthropogenic sulfur and nitrogen contamination in the Sichuan Basin, China. *Geochem. J.* **2006**, *40*, 309–332. [[CrossRef](#)]
50. Yan, Z.; Han, X.; Yue, F.-J.; Zhong, J.; Wang, Z.-J.; Zeng, J.; Li, S.-L. Aquatic chemistry and sulfur isotope composition of precipitation in a karstic agricultural area, Southwest China. *Earth Environ.* **2019**, *47*, 811–819. (In Chinese)
51. Gan, C. Geological characteristics and genetic investigation of the Maochang type pyrite deposits. *Miner. Depos.* **1985**, *4*, 51–57. (In Chinese)
52. Das, A.; Pawar, N.J.; Veizer, J. Sources of sulfur in Deccan Trap rivers: A reconnaissance isotope study. *Appl. Geochem.* **2011**, *26*, 301–307. [[CrossRef](#)]